

Adversarial Detection: Attacking Object Detection in Real Time

Han Wu, Syed Yunas, Sareh Rowlands, Wenjie Ruan, and Johan Wahlstrom*

Abstract—Intelligent robots hinge on accurate object detection models to perceive the environment. Advances in deep learning security unveil that object detection models are vulnerable to adversarial attacks. However, prior research primarily focuses on attacking static images or offline videos. It is still unclear if such attacks could jeopardize real-world robotic applications in dynamic environments. There is still a gap between theoretical discoveries and real-world applications. We bridge the gap by proposing the first real-time online attack against object detection models. We devised three attacks that fabricate bounding boxes for nonexistent objects at desired locations. The demo video is available at [url].

I. INTRODUCTION

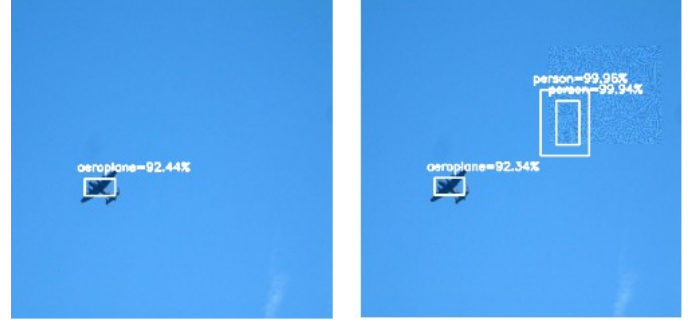
A reliable object detection model is crucial for some safety-critical robotic applications. For example, a modular autonomous driving system relies on object detection models to perceive the environment. Advances in deep neural networks bring a leap toward high-accuracy detection models, but the breakthrough also introduces potential vulnerabilities: deep neural networks are vulnerable to adversarial attacks.

In 2014, Goodfellow et al. fooled an image classification model by adding a human unperceivable perturbation to the entire input image [1]. The imperceptibility added constraints on the strength of the attack. Later, Brown et al. no longer restricted their attacks to imperceptible changes. Instead, they designed an adversarial patch that can be printed out in the physical world [2]. The physical patch fooled an image classification model to misclassify the most salient object in the image. However, the attack against image classification models cannot fool object detection models. In 2018, Liu et al. introduced the DPatch, a digital patch that fooled an object detection model [3], and Lee et al. further extended the attack to be a physical patch in 2019 [4].

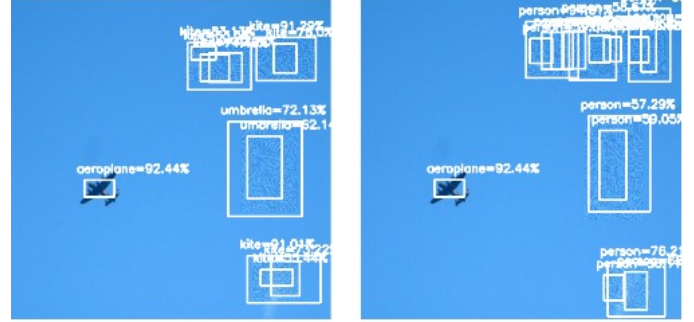
It is still unclear how we can generate the adversarial patch to attack a real-time robotic application. Training a robust physical patch takes a long time to optimize over the training set, and the physical patch is susceptible to variations in camera distance and angle. Real-world robotic applications sit in a dynamic environment. The input image for the object detection models is not guaranteed to be captured within a valid distance and from specific angles for physical attacks.

Recent research in penetration tests against the Robot Operating System (ROS) gives us some insights [5]. Dieber et al. succeeded in isolating a ROS node so that they could intercept and manipulate the ROS message that contains sensor data while the victim node is unaware of the attack.

Han Wu, Sareh Rowlands and Johan Wahlstrom are with the University of Exeter, Stocker Rd, Exeter EX4 4PY, the UK (hw630@exeter.ac.uk; s.rowlands@exeter.ac.uk; j.wahlstrom@exeter.ac.uk).



(a) The **original image** (left) only contains an aeroplane. The **One-Targeted Attack** (right) generates one patch containing several target objects (person).



(b) The **Multi-Untargeted Attack** (left) generates multiple patches containing different kinds of objects (aeroplane, kite, umbrella). The **Multi-Targeted Attack** (right) generates multiple patches containing several target objects (person).

Fig. 1: We can generate adversarial overlays of arbitrary shapes at specified positions in real time.

As a result, it is possible to inject digital patches into the ROS message that contains the camera image. Our research generates digital patches at desired locations in real time and then can exploit the vulnerability to inject the digital patches into the input image. Overall, this paper makes the following contributions:

- We devised three adversarial attacks that can generate digital patches of different shapes at specified locations in real time (see Figure 1).
- We further investigated the adversarial effect of digital patches of different sizes and aspect ratios.
- We tested our attacks in the Robot Operating System (ROS). The system is open-sourced on Github for future research¹.

¹The code is available on Github: <https://github.com/wuhanstudio/adversarial-detection>

II. PRELIMINARIES

This section clarifies the differences between adversarial filters and adversarial patches. Then we introduce how prior research applies them in the digital and physical world. Our research focuses on applying adversarial patches in the digital world.

A. The Adversarial Filter

The adversarial filter refers to the perturbation added to the entire image. Thus, the adversarial filter is the same size as the input image and is unperceivable by human eyes. According to how we apply the perturbation, adversarial filters consist of digital and physical filters.

1) **Digital Filter** (Figure 2a): The first adversarial attack against image classification models is a digital filter that adds a small perturbation to the entire input image [1]. We can either generate the perturbation using gradient-based methods [8] [9] or optimization-based methods [10]. Prior research uses the l_1 , l_2 , and l_∞ norm to measure the human perceptual distance between the adversarial and the original input image.

The digital filter proves the existence of adversarial examples but has its limitations in practical attacks if we do not have access to the input image.

2) **Physical Filter** (Figure 2b): The physical filter removes the limitation of the digital filter by attaching a translucent film to the camera lens [7] to perturb the entire image. The physical filter is more practical than the digital filter attack because it only requires physical access to the camera to initiate the attack.

However, it is challenging to manufacture a film that precisely replicates the adversarial perturbation. Thus, reproducing the adversarial filter in the physical world is still an unsolved problem in the research area. Besides, to the best of our knowledge, we only see physical filters that attack image classification models that classify the most salient object in the image.

B. The Adversarial Patch

Under some scenarios, adding a conspicuous perturbation to a small region of the input image is not a concern. We can generate distinguishable adversarial patches by removing the constraint on the perceivability of the perturbation. In addition, we add constraints on the patch size.

Besides, if we use the adversarial filter to attack an object detection model, we cannot precisely control the location of falsified objects because the filter perturbs the entire image. Similarly, adversarial patches consist of digital patches and physical patches.

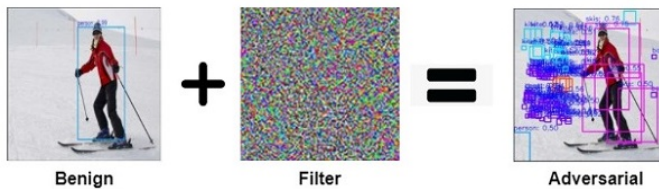
1) **Digital Patch** (Figure 3a): In 2018, Liu et al. designed the DPatch [3] to attack the Faster R-CNN object detection model [11]. The DPatch is location-independent, which means it can be placed anywhere in the input image. In 2020, Chow et al. proposed the TOG attack that could generate a 40x40 adversarial patch to fool an object detection model to misclassify objects to which the patch is attached.

2) **Physical Patch** (Figure 3b): In 2017, landmark research by Google generated a physical patch to attack an image classification model [2]. Later, research interests gradually shifted to physical patch, because it is easy to carry out in the real world. Lee et al. [4] and Wang et al. [6] extended the physical patch attack from image classification to object detection.

However, physical patches are inflexible: once the adversarial patch is printed out, we cannot change it. To improve its flexibility, Hoory et al. dynamically displayed adversarial patches on a flat screen attached to a car [12].

C. Summary

In the research area of adversarial attacks, it is common to design digital perturbations first. Later research will extend the digital attack to the physical world. In the next section, we introduce how we generate unperceivable digital patches at desired locations in real time.



(a) The Digital Filter applies the perturbation to the entire input image in the digital world [6].



(b) The Physical Filter applies the perturbation by attacking the camera lens, e.g., a translucent film attached to the camera lens [7].



(a) The Digital Patch replaces a part of the input image with the adversarial patch (left up corner) [3].



(b) The Physical Patch prints the adversarial patch on a physical object, e.g., on a poster [4].

Fig. 2: The Adversarial Filter perturbs the entire image.

Fig. 3: The Adversarial Patch perturbs part of the image.

III. ADVERSARIAL DETECTION

Our objective is to fool the YOLOv3 [13], and YOLOv4 [14] object detection models to mistakenly detect objects at locations where there is no object. We generate adversarial overlays by combining adversarial filters' imperceptibility and adversarial patches' localizability.

A. Problem Formulation

The YOLO object detection model splits the input image into $S \times S$ grids and makes predictions for each grid. For example, the input shape of YOLO is 416x416x3 (height, width, and channel). If $S = 13$, we divide each channel into 13×13 grids, and each grid is 32×32 pixels.

To detect objects of different sizes, YOLO makes predictions at three different scales (see Figure 4). The first, second, and third output layer contains 13×13 , 26×26 , and 52×52 grids, respectively. The first output layer detects large objects, and the third output layer detects small objects.

Besides, YOLO pre-defined three anchor boxes ($B = 3$) at each scale to detect objects of different aspect ratios. Thus, we have 9 pre-defined anchor boxes for 3 scales.

Lastly, each output contains the shape and location of the bounding box, the confidence value, and the probability vector for each class (see Figure 4). If the model is pretrained on the MS COCO dataset [15] that contains 80 classes ($K=80$), each output contains 85 values consisting of 4 dimensions (b_x, b_y, b_w, b_h), 1 confidence value (c), and 80 probabilities (p_1, p_2, \dots, p_{80}) for each class.

Putting things together: Given an input image x , the object detection model outputs $S \times S \times B$ candidate bounding boxes $o \in \mathcal{O}$ at three different scales ($S \in \{13, 26, 52\}, B = 3$). Each candidate box o contains ($b_x, b_y, b_w, b_h, c, p_1, p_2, \dots, p_K$) for K classes. For example, the size of the first output layer is $(13, 13, 3, 85)$. The image is divided into 13×13 grids, and the model makes predictions for 3 anchor boxes. Each prediction contains 85 values ($85 = 4 + 1 + 80$).

The adversarial attack aims to generate an adversarial perturbation $\delta \in [-1, 1]^{whc}$ bounded by the l_p norm, such that the adversarial output $\hat{\mathcal{O}}(x')$ is different from the original output $\hat{\mathcal{O}}(x)$.

$$\min ||x' - x||_p \quad s.t. \quad \hat{\mathcal{O}}(x') \neq \hat{\mathcal{O}}(x)$$

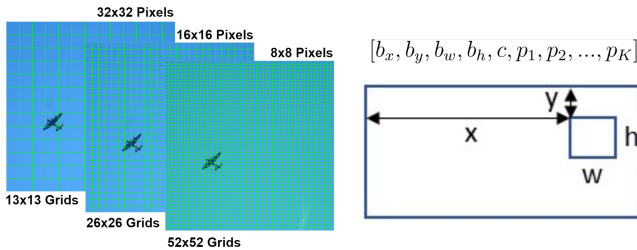


Fig. 4: The YOLO object detection model makes predictions at three scales.

B. The Adversarial Overlay

As introduced in the last section, adversarial filters are imperceptible to human eyes but cannot precisely control where we fabricate objects. On the other hand, adversarial patches are pinpointable but conspicuous.

Thus we devise a new method, the adversarial overlay, that applies an imperceptible perturbation to part of the image. The equation (3) below defines how adversarial overlay applies the perturbation δ via a binary mask $m \in \{0, 1\}^{wh}$.

$$\begin{aligned} x'_{filter} &= x + \delta \\ x'_{overlay} &= x + m \odot \delta \\ x'_{patch} &= (1 - m) \odot x + m \odot \delta \end{aligned}$$

The \odot operation represents the Hadamard operator performing element-wise multiplication, so that we can decide where to apply the perturbation.

The adversarial filter x'_{filter} applies the perturbation to the entire image without the mask m . The adversarial patch x'_{patch} utilizes the mask to replace part of the image. The adversarial overlay applies the mask to the perturbation and adds it as an overlay to the original image.

Besides, we propose three adversarial loss functions that can efficiently generate the perturbations in real time: one-targeted attack, multi-targeted attack, and multi-untargeted attack. The function $\sigma(x)$ below represents the sigmoid function.

$$\begin{aligned} \text{One Targeted: } \mathcal{L}_1(\mathcal{O}) &= \sum_{1 \leq i \leq |\mathcal{O}|} \max [\sigma(c^i) * \sigma(p_t^i)] \\ \text{Multi Targeted: } \mathcal{L}_2(\mathcal{O}) &= \sum_{i=1}^S \sum_{j=1}^{|\mathcal{O}|} [\sigma(c^i) * \sigma(p_t^i)] \\ \text{Multi Untargeted: } \mathcal{L}_3(\mathcal{O}) &= \sum_{i=1}^S \sum_{j=1}^{|\mathcal{O}|} \sum_{k=1}^K [\sigma(c^i) * \sigma(p_k^i)] \end{aligned}$$

We notice that the output bounding box o contains the confidence value c and one-hot encoding $[p_1, p_2, \dots, p_K]$ for the probability of each class. The confidence value and the probability vector collectively determine whether or not a bounding box is drawn on the output image. Thus, by maximizing the product of confidence and probability vector, we can fabricate objects at desired locations.

$$o^i = [b_x^i, b_y^i, b_w^i, b_h^i, c^i, p_1^i, p_2^i, \dots, p_K^i], \quad 0 \leq i \leq |\mathcal{O}|$$

The one-targeted attack generates one overlay that contains the target object $t \in [0, K]$ by finding the bounding box with the maximum value of the product $\sigma(c^i) * \sigma(p_t^i)$. This method generates only one overlay that contains target objects because we increase the confidence and probability of the maximum one in all output bounding boxes.

The multi-targeted attack generates multiple overlays that contain target objects $t \in [0, K]$ by maximizing the sum of $\sigma(c^i) * \sigma(p_t^i)$ for the target class.

Algorithm 1 The Adversarial Overlay Attack

Input: The object detection model $f(\theta, x)$, a mask m that defines a series of locations where we generate false positive bounding boxes

Parameters: the number of iterations n , the learning rate α , and the strength of the attack ξ measured by l_∞ norm.
Output: adversarial perturbation δ .

Initialization:

if monochrome **then**

$\delta \leftarrow 0^{416 \times 416}$

else

$\delta \leftarrow 0^{416 \times 416 \times 3}$

end if

for each input image x **do**

$x' = x$

for each iteration **do**

Overlay: $x' = x' + m \odot \delta$

Gradient: $\nabla = \frac{\partial \mathcal{L}_{adv}(\mathcal{O})}{\partial x'}$

if monochrome **then**

$\delta = \delta + \frac{1}{3}\alpha(\nabla_R + \nabla_G + \nabla_B)$

else

$\delta = \delta + \alpha \text{sign}(\nabla)$

end if

$\delta = \text{clip}(\delta, -\xi, \xi)$

$x' = \text{clip}(x', 0.0, 1.0)$

end for

end for

The multi-untargeted attack generates multiple overlays that contain different objects by maximizing the sum of $\sigma(c^i) * \sigma(p_t^i)$ for all classes.

In addition, we can generate monochrome greyscale overlays. Greyscale overlays add the same value to each channel, making the perturbation less conspicuous. We can generate monochrome overlays using the average of the Red, Green, and Blue channels or from a single channel since human eyes are most sensitive to the green channel.

At the end of each iteration, we clip the value of the perturbation so that it does not exceed the pre-defined boundary. The adversarial image of the original DPatch [3] contains invalid negative pixel values. Thus, we also clip the value of the adversarial image to make sure it is still a valid image. We summarize our method in Algorithm 1.

C. System Architecture

We design an adversarial detection system to attack the YOLO object detection model. The system adopts a modular design pattern so that we can test our methods in different environments (see Figure 5) using the same architecture. The system consists of three components: the Data Source, the Server, and the Control Panel.

The Data Source: The data source publishes the input image to the server. We can publish the image from different sources, including the PC camera, the ROS Gazebo Simulator, and a real Turtlebot 3.

The Server: The server receives the input image stream from the data source via WebSocket connections. Meanwhile, it obtains the adversarial mask from the control plane. Then the server generates and injects the adversarial overlay into the input image. Besides, the YOLO object detection model is deployed on the server.

The Control Plane: The control plane is a website where the attacker can draw the mask at arbitrary locations. The browser sends the mask to the server via WebSocket connections.

We used YOLO object detection models pre-trained on the MS COCO dataset for the PC environment. Besides, we trained two traffic sign detection models for the ROS Gazebo and the ROS Turtlebot environment to validate our attacks.

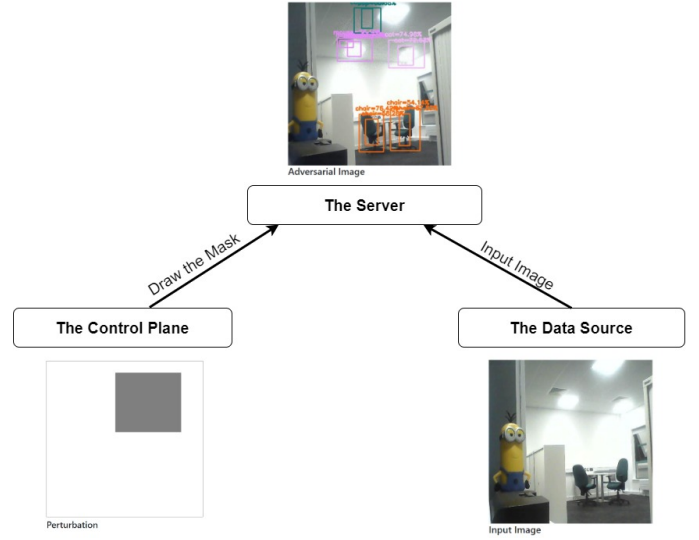


Fig. 6: Adversarial Detection: System Architecture

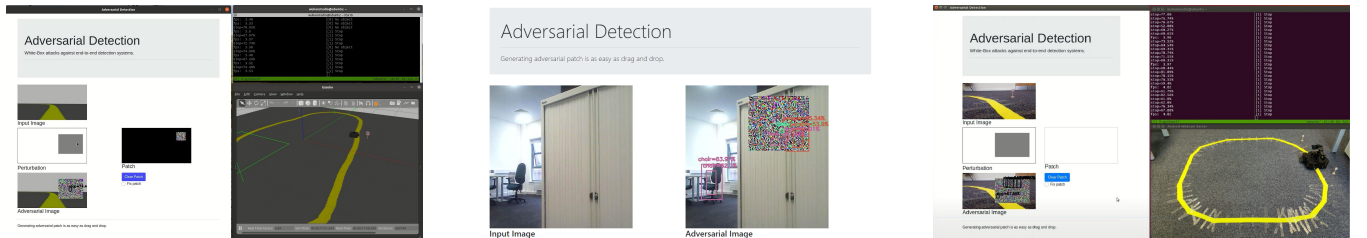


Fig. 5: We tested our attack in three environments. Here we made the overlay visible for illustration purposes.

IV. EXPERIMENTAL RESULTS

A. Evaluation Metrics

Prior research uses the Mean Accuracy Precision (mAP) [16] to evaluate the accuracy of object detection models. However, the objective of our attack is to fabricate new bounding boxes but not to decrease the accuracy of existing objects. The evaluation metrics need to reflect the efficiency of generating new bounding boxes in real time.

Besides, the mAP evaluation metric requires access to the ground truth, which is human-labeled bounding boxes. The online attack that fools the object detection system in real time do not have access to the ground truth. It is impossible to have humans label the video stream in real time.

As a result, we use two evaluation metrics that evaluate the efficiency of generating new objects and do not need access to the ground truth.

1) **Success Rate:** The success rate measures the percentage of images we successfully fooled within a short period. For a real-time online attack, we need to achieve a satisfying success rate within a limited number of iterations.

2) **Mean Box Number Increase:** We measure the number of new bounding boxes generated compared to the benign output. The more bounding boxes we generate, the stronger the perturbation is. But fabricating more objects requires more iterations.

We need to find the minimum number of iterations required to achieve a satisfying success rate and fabricate enough bounding boxes. The PASCAL VOC-2012 validation set is used in the following experiments.

B. Hyper-parameters

Three hyper-parameters are crucial for the attack: the attack strength ξ , the step size α , and the box size. Since we can generate less conspicuous monochrome overlays, we further investigated the effect of using gradients from different channels. Besides, we examined if the adversarial perturbation is susceptible to different aspect ratios.

1) **The Attack Strength:** The attack strength ξ puts a boundary on the maximum perturbation added to each pixel. A larger ξ makes the attack stronger but results in a more conspicuous perturbation.

In Figure 7a, $\xi \in \{10, 8\}$ achieves much higher success rates than $\xi \in \{4, 2\}$ after 100 iterations. Though $\xi = 10$ and $\xi = 8$ share similar success rates, $\xi = 10$ generates more bounding boxes than $\xi = 8$ (see Figure 8a).

For a real-time attack, we aim to generate at least one bounding box in 30 iterations, both $\xi = 10$ and $\xi = 8$ satisfy the requirement. We think $\xi = 8$ finds a good balance between the attack strength and the impermeability of the perturbation.

2) **The Step Size:** The step size α controls how fast we update the perturbation at each step. A larger α could fabricate bounding boxes in fewer iterations but make the update more unstable.

In Figure 7b, both $\alpha = 1$ and $\alpha = 2$ achieve more than 90% success rate in 30 iterations, and $\alpha > 4$ deteriorates the success rate. In Figure 8b, $\alpha = 1$ eventually generates more bounding boxes than $\alpha = 2$, but for a real-time online attack, it's more preferable to have a faster attack.

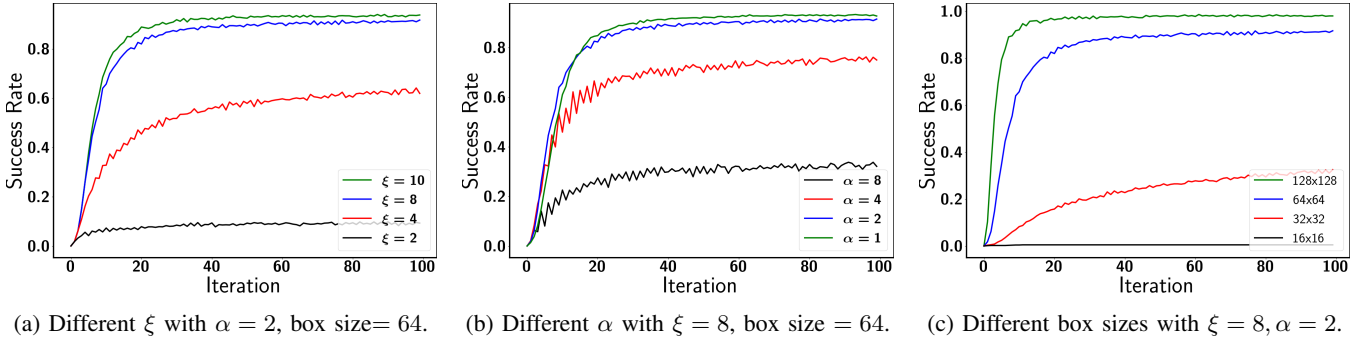


Fig. 7: The success rate of the multi-untargeted attack with different ξ , α , and box sizes.

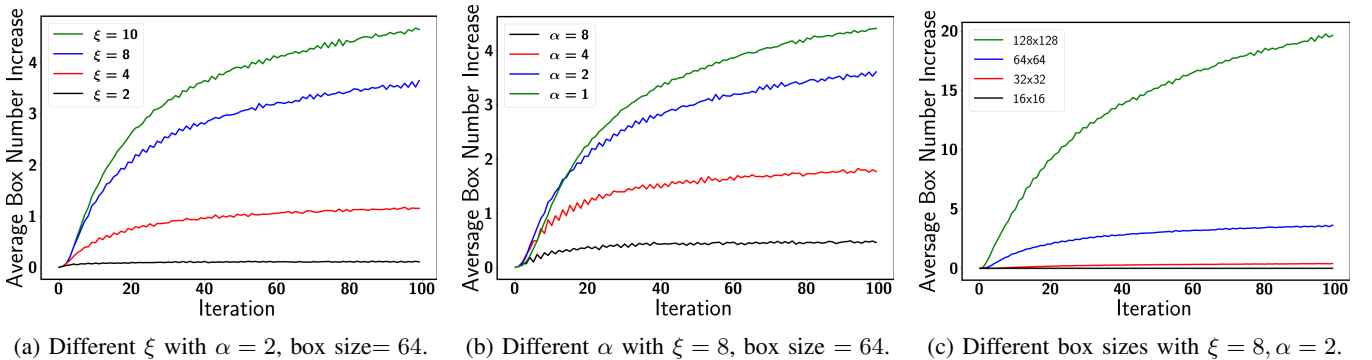


Fig. 8: The average box number increase of the multi-untargeted attack with different ξ , α , and box sizes

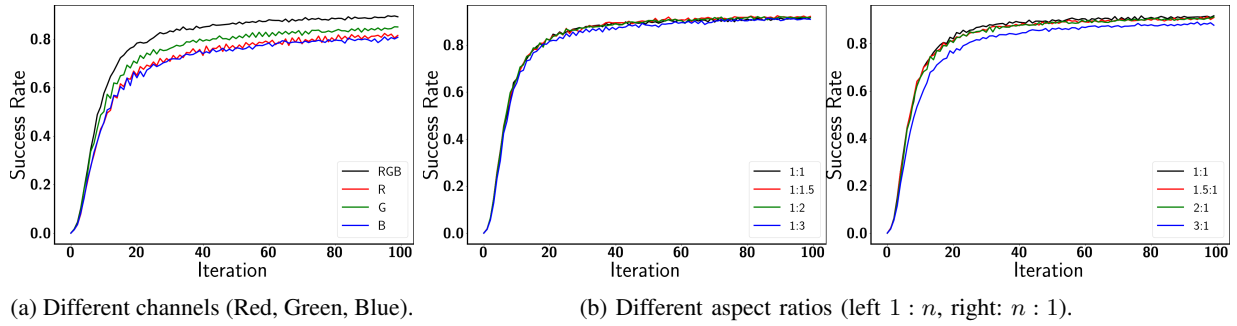


Fig. 9: The success rate of the multi-untargeted attack with different channels and aspect ratios.

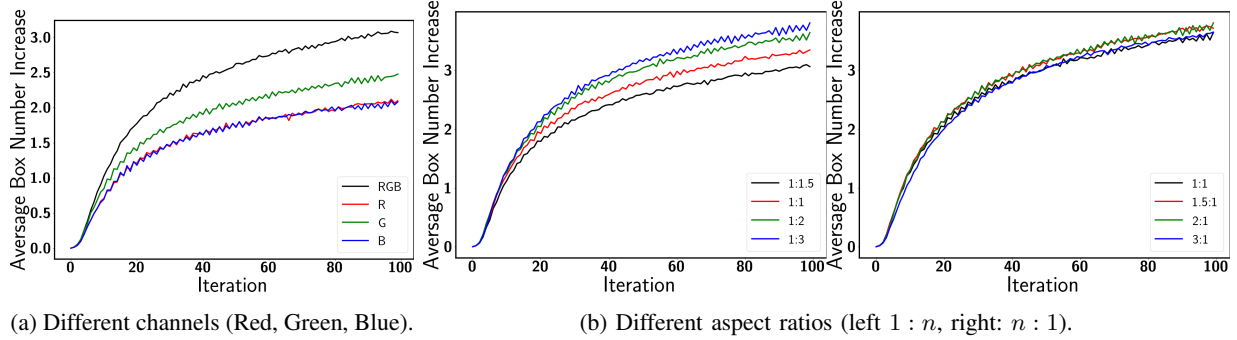


Fig. 10: The average box number increase of the multi-untargeted attack different channels and aspect ratios.

3) **The Box Size:** The box size determines the total number of pixels we can perturb. The more pixels we can manipulate, the easier it is to deviate the model output from original predictions. We need to find the minimum box size for our attack.

In Figure 7c, the box size of both 128×128 and 64×64 achieve 90% success rate after 30 iterations, while the box size of 32×32 struggles to achieve successful attacks. And the box size smaller than 16×16 is unable to attack the model with $\xi = 8$ and $\alpha = 2$. Besides, as expected, the larger the box size is, the more bounding boxes the attack can generate (see Figure 8c). For a real-time online attack, we suggest the overlay box size to be at least 64×64 .

4) **The Monochrome Channel:** For the attack that generates a polychrome overlay, we update each channel of the perturbation using the gradients of each channel, respectively. While for the monochrome overlay, we should decide which color channel we prioritize.

Interestingly, the experimental results (see Figure 9a and 10a) show that the object detection model is more sensitive to the green channel, as we humans are more sensitive to green light. Using the average gradient of RGB channels, we achieve the highest success rate and generate the most number of boxes.

5) **The Aspect Ratio:** Our attack can generate adversarial overlays of arbitrary shapes. Thus we can study if the object detection model is more susceptible to adversarial overlays of specific aspect ratios, e.g., wide (1:n) or long (n:1) boxes. For a fair comparison, overlay boxes of different aspect ratios have the same area (the same number of pixels perturbed).

In Figure 9b, different aspect ratios do not cause observable dissimilarities in success rates. In Figure 10b, though the aspect ratio 1 : 3 generates more bounding boxes than 1 : 1.5 after 100 iterations, this attributes to a slightly more number of boxes perturbed ($1 : 3 \rightarrow 37 \times 111 = 4108$, $1 : 1.5 \rightarrow 52 \times 78 = 4056$). Thus we cannot conclude the aspect ratio has a discernible impact on the attack.

As a result, we use $\xi = 8$, $\alpha = 2$, and box size = 64×64 as default values for our attack, and the monochrome overlay uses the average of gradients from RGB channels. Besides, the aspect ratio does not show an evident effect on the adversarial attacks.

V. CONCLUSIONS

In conclusion, we demonstrate that it is possible to attack an object detection system in real time. We can generate human unperceivable adversarial overlays of arbitrary shapes to fabricate bounding boxes at desired locations.

In the future, we plan to investigate the effect of the attack on modular autonomous driving systems that rely on object detection models to perceive the environment. Besides, we will explore how to detect adversarial attacks so that we can embrace deep learning models in safety-critical robotic applications in a safe way.

ACKNOWLEDGMENT

The project is supported by Offshore Robotics for Certification of Assets (ORCA) Partnership Resource Fund (PRF) on Towards the Accountable and Explainable Learning-enabled Autonomous Robotic Systems (AELARS) [EP/R026173/1].

REFERENCES

- [1] I. J. Goodfellow, J. Shlens, and C. Szegedy, "Explaining and harnessing adversarial examples," *arXiv preprint arXiv:1412.6572*, 2014.
- [2] T. Brown, D. Mane, A. Roy, M. Abadi, and J. Gilmer, "Adversarial patch," *arXiv preprint arXiv:1712.09665*, 2017.
- [3] X. Liu, H. Yang, Z. Liu, L. Song, H. Li, and Y. Chen, "Dpatch: An adversarial patch attack on object detectors," *arXiv preprint arXiv:1806.02299*, 2018.
- [4] M. Lee and Z. Kolter, "On physical adversarial patches for object detection," *arXiv preprint arXiv:1906.11897*, 2019.
- [5] B. Dieber, R. White, S. Taurer, B. Breiling, G. Caiazza, H. Christensen, and A. Cortesi, "Penetration testing ros," in *Robot operating system (ROS)*. Springer, 2020, pp. 183–225.
- [6] D. Wang, C. Li, S. Wen, Q.-L. Han, S. Nepal, X. Zhang, and Y. Xiang, "Daedalus: Breaking nonmaximum suppression in object detection via adversarial examples," *IEEE Transactions on Cybernetics*, 2021.
- [7] J. Li, F. Schmidt, and Z. Kolter, "Adversarial camera stickers: A physical camera-based attack on deep learning systems," in *International Conference on Machine Learning*. PMLR, 2019, pp. 3896–3904.
- [8] A. Madry, A. Makelov, L. Schmidt, D. Tsipras, and A. Vladu, "Towards deep learning models resistant to adversarial attacks," in *6th International Conference on Learning Representations, ICLR 2018, Vancouver, BC, Canada, April 30 - May 3, 2018, Conference Track Proceedings*, 2018.
- [9] A. Kurakin, I. J. Goodfellow, and S. Bengio, "Adversarial examples in the physical world," in *Artificial intelligence safety and security*. Chapman and Hall/CRC, 2018, pp. 99–112.
- [10] N. Carlini and D. Wagner, "Towards evaluating the robustness of neural networks," in *2017 IEEE Symposium on Security and Privacy (SP)*. Ieee, 2017, pp. 39–57.
- [11] S. Ren, K. He, R. Girshick, and J. Sun, "Faster r-cnn: Towards real-time object detection with region proposal networks," *Advances in neural information processing systems*, vol. 28, 2015.
- [12] S. Hoory, T. Shapira, A. Shabtai, and Y. Elovici, "Dynamic adversarial patch for evading object detection models," *arXiv preprint arXiv:2010.13070*, 2020.
- [13] J. Redmon and A. Farhadi, "Yolov3: An incremental improvement," *arXiv preprint arXiv:1804.02767*, 2018.
- [14] A. Bochkovskiy, C.-Y. Wang, and H.-Y. M. Liao, "Yolov4: Optimal speed and accuracy of object detection," *arXiv preprint arXiv:2004.10934*, 2020.
- [15] T.-Y. Lin, M. Maire, S. Belongie, L. Bourdev, R. Girshick, J. Hays, P. Perona, D. Ramanan, C. L. Zitnick, and P. Dollár, "Microsoft coco: Common objects in context," 2014.
- [16] J. Cartucho, R. Ventura, and M. Veloso, "Robust object recognition through symbiotic deep learning in mobile robots," in *2018 IEEE/RSJ International Conference on Intelligent Robots and Systems (IROS)*, 2018, pp. 2336–2341.